Effects of single vacancy defects on 1/f noise in graphene/h-BN FETs

Ting Wu[1], Abdullah Alharbi[1], Takashi Taniguchi[2], Kenji Watanabe[2], Davood Shahrjerdi[1,3]
[1]*Electrical and Computer Engineering Department, New York University, Brooklyn, NY, 11201*
[2]*National Institute of Materials Science, 1-1 Namiki Tsukuba, Ibaraki 305-0044, Japan*
[3]*Center for Quantum Phenomena, Physics Department, New York University, New York, NY 10003*
Email: davood@nyu.edu

Overview: sp^2 carbon materials, including carbon nanotubes and graphene, have been used extensively for making highly sensitive biochemical field-effect transistor (FET) sensors. Previous studies suggest that structural disorders in these materials enhance the device sensitivity. Despite many studies on device sensitivity in relation to structural defects, only a few studies have examined the effect of defects on low-frequency noise in graphene FETs [1]. However, no study has yet investigated the correlation between the specific type defects, *e.g.* single vacancy defects, and the low-frequency noise characteristics of graphene transistors. Here, we systematically study the connection between the concentration of single vacancy defects, the low-frequency noise and carrier transport in graphene FETs.

Experiment and Results: Fig. 1a shows the summary of key processing steps. We fabricated graphene transistors with a global bottom gate on SiO_2/Si substrates. To remove the possible effects of SiO_2 on the 1/f noise of the device (due to charge trapping or long-range Coulomb scattering), we inserted a thin h-BN flake between the graphene and SiO_2 films. To improve the graphene/h-BN interface, we performed ultrahigh vacuum annealing after the stacking process. Figs. 1b-c show the optical image and the schematic illustration of the four-point graphene/h-BN transistor.

To produce single vacancy defects, we irradiated the graphene FETs with low-energy Ar^+ ions at 90 eV. Previous studies have shown that this ion energy generates mostly single vacancies in graphene [2]. To systematically study the link between the vacancy concentration and the key device metrics (noise, mobility and residual carrier concentration), we used the same device for all electrical and noise measurements and sequentially increased its defect density. We used Raman spectroscopy (Fig. 2) to quantify the density of vacancies (n_D) in graphene [3].

In Fig. 3, we plotted the intrinsic channel resistance of a graphene FET at four different vacancy concentrations. The data indicate the monotonic increase of the channel resistance with increasing the defect concentration, hinting at the degradation of mobility in the graphene channel. We then extracted the carrier mobility μ and the residual carrier concentration n_0 using the method described in [4]. Fig. 4 shows the summary of our calculations, indicating the monotonic decrease of μ because of the sequential Ar^+ irradiation of the graphene FET.

Next, we measured the low-frequency noise of the graphene FET as a function of the gate bias after each irradiation. From these measurements, we observed that the noise amplitude *vs.* gate bias curve measured at each defect density exhibits a V-shape profile (data not shown), suggesting the dominance of short-range disorder scattering in graphene [5]. Fig. 5 shows the normalized current noise spectral density, S_I/I^2, at the Dirac point for different defect densities. Despite the gradual increase of the defect density in the graphene channel, we found out that S_I/I^2 remains unchanged. To understand the physical origin of this noise behavior, we use the mobility fluctuation model. In this model, $S_I/I^2 \propto N_t^{\mu}.l_0^2$, where N_t^{μ} is the concentration of the scattering centers and l_0 is the mean free path of the carriers (*i.e.* proportional to mobility). Looking closely at the transport data (Fig. 4), we found that the mobility in our irradiated graphene exhibits the following relation: $\mu_2/\mu_1 \cong \sqrt{n_{D2}/n_{D1}}$. From this observation together with the unchanged S_I/I^2 curves, we conclude that all vacancy defects in our Ar-irradiated graphene devices act as the scattering centers and contribute to 1/f noise. Fig. 6 shows the noise amplitude and drain current at the Dirac point *vs.* the vacancy defect concentration, indicating the reduction of the noise amplitude commensurate with I_D.

Conclusions: The combination of transport and noise studies reveals that the mobility fluctuation model can fully explain the 1/f noise behavior of the graphene films containing only single vacancy defects. Our study, for the first time, establishes that the single vacancies in graphene act as the scattering centers and directly contribute to 1/f noise.

This research used resources of the CFN, which is a U.S. DOE Office of Science Facility, at Brookhaven National Laboratory under Contract No. DE-SC0012704. We acknowledge financial support by NSF-CMMI award #1728051.

[1] M. Hossain *et al*., *Appl. Phys. Lett*., vol. 102, p. 153512, (2013). [2] O. Lehtinen *et al*., *Phys. Rev. B*, vol. 81, p. 153401, (2010).
[3] L. G. Cancado *et al*., *Nano Lett*., vol. 11, p. 3190-3196 (2011). [4] K. Seyoung *et al*., *Appl. Phys. Lett*., vol. 94, p. 06217 (2009).
[5] Y. Zhang, *et al*., *ACS Nano*, vol. 5, p. 8124–8130 (2011).

978-1-5386-3028-0/18/$31.00 ©2018 IEEE

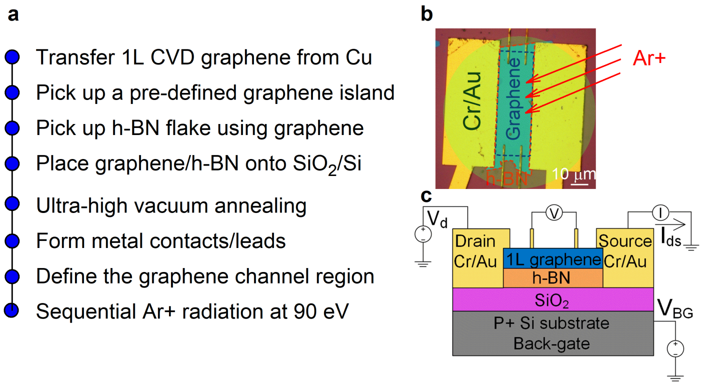

Fig. 1: (a) Key fabrication steps of the graphene/h-BN FETs. (b) Optical image of the final four-point structure. Multiple steps of low energy Ar^{+} irradiation were performed to introduce different densities of single vacancies in the graphene channel. (c) Schematic illustration of the measurement setup.

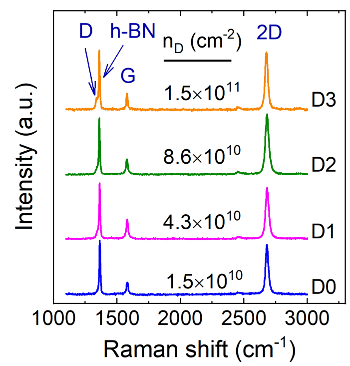

Fig. 2: Raman spectra of the graphene/hBN channel after each irradiation step. The corresponding density of vacancy defects are given on each curve.

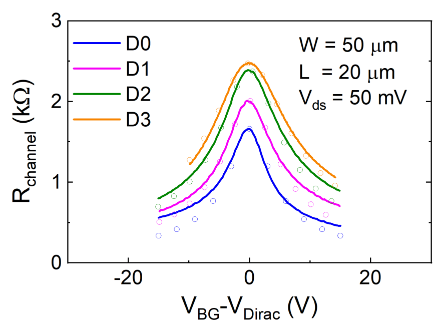

Fig. 3: Intrinsic channel resistance of the graphene/h-BN FET as a function of the back-gate voltage measured after each irradiation step. The solid lines represent the measured results and the open circles represent the fitted data.

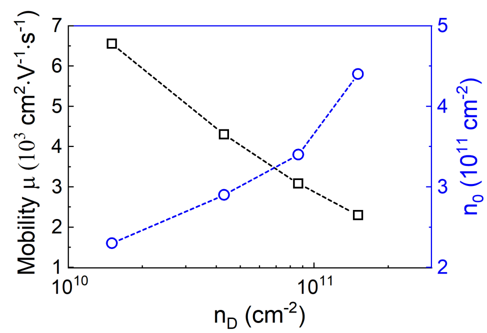

Fig. 4: Carrier mobility µ and the residual carrier concentration n_0 *vs.* defect density n_D. The lines are guide to the eye.

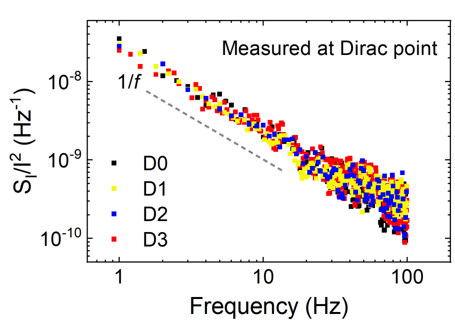

Fig. 5: Normalized current noise spectral density S_I/I^2 at the Dirac point measured after each irradiation step. The S_I/I^2 remains unchanged at various irradiation levels. Mobility fluctuation model can fully explains this trend.

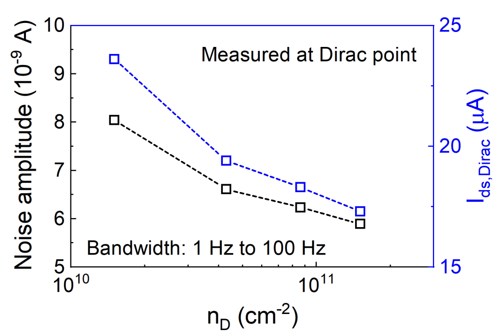

Fig. 6: Noise amplitude and drain current at the Dirac point *vs.* concentration of vanacy defects n_D. Noise amplitude decreases in proportion to $I_{ds,Dirac.}$